Charged-current quasielastic neutrino scattering from ^{12}C in an extended superscaling model with two-nucleon emission

V. L. Martinez-Consentino* and J. E. Amaro†

Departamento de Física Atómica, Molecular y Nuclear, Universidad de Granada, E-18071 Granada, Spain
and Instituto Carlos I de Física Teórica y Computacional, Granada, Spain

(Received 29 August 2023; accepted 28 November 2023; published 18 December 2023)

The quasielastic cross section of charged-current neutrino and antineutrino scattering on ^{12}C is calculated using an improved superscaling model with relativistic effective mass. Our model encompasses two-particle emission induced by neutrinos, which we distinguish into two contributions. The first contribution arises from meson-exchange currents, and its calculation is performed at a microscopic level. The second contribution is phenomenological and extracted from the high-energy tail of the scaling function, assumed to be produced by 2p2h mechanisms where the one-body current plays a role, such as short-range correlations and interferences with MEC, final-state interaction, etc. The model explicitly includes the modification of the relativistic effective mass of the nucleon within the relativistic mean field model of nuclear matter. The meson exchange currents are also consistently calculated within the same model. With this model, we present predictions for the neutrino and antineutrino cross sections of ^{12}C that have been measured in accelerator experiments.

DOI: 10.1103/PhysRevD.108.113006

I. INTRODUCTION

Neutrino interactions with nuclei are of vital importance for a series of experiments ongoing and planned in the near future [1]. In recent years, a large experimental program focused on accelerator-based neutrino oscillation experiments has been developed. The primary objective of this program is to enhance our understanding of neutrino properties by accurately measuring the oscillation parameters and investigating the weak CP-violating phase. These measurements are crucial for elucidating the enigmatic phenomena surrounding neutrino oscillations and their fundamental role in the realm of particle physics. The majority of long-baseline neutrino experiments employ complex nuclear targets, making it crucial to have excellent control over medium effects in neutrino-nucleus scattering to achieve precise measurements of neutrino oscillation parameters [2–4].

The cross section of neutrino-nucleus scattering for the energies of interest, which are essential for these experiments [5,6], is made up of various channels, including quasielastic interactions but the nuclear models present uncertainties [7,8] related to the presence of processes, such as final-state interactions, multinucleon emission, pion emission and other inelasticities that limit the accuracy of oscillation experiments [9–13]. Efforts to reduce uncertainties in neutrino-nucleus scattering models include measuring the proton or neutron multiplicity of final states [11,14–16].

The inclusive (e, e') cross sections of nuclei provide a useful starting point for modeling neutrino-nucleus interactions. The isovector component of the electromagnetic nuclear responses can be related to the vector component of the weak charged-current responses that contribute to the neutrino cross sections. Therefore, the systematic differences observed between theoretical predictions of neutrino cross sections should be closely associated with differences in the description of (e, e') data [17–22].

In this work, we present predictions for neutrino quasielastic cross sections based on an extended superscaling model that has been tuned from inclusive electron scattering data. It is based on the superscaling analysis with relativistic effective mass (SuSAM*) model of Refs. [23,24], modified to accommodate the possibility of a contribution that partially violates scaling. This modification acknowledges that the inclusive quasielastic (QE) cross section data exhibit deviations from strict scaling behavior.

The original SuSAM* model differs from the superscaling analysis (SuSA) model [25–28] in that it is based on the relativistic mean-field model (RMF) of nuclear matter and thus contains, by construction, nucleon medium effects encoded in a relativistic effective mass for the nucleon.

Our modified SuSAM$*$+2p2h model is made up of three contributions: (i) the purely quasielastic cross section (1p1h); (ii) the two-particle two-hole (2p2h) emission

*victormc@ugr.es
†amaro@ugr.es

channel from a theoretical model of meson-exchange currents (MEC); and (iii) an additional phenomenological 2p2h tail contribution attributed to short-range correlations (SRC), interference with MEC, final-state interactions (FSI) and other processes partially contributing to the scaling function, exhibiting slight deviations from scaling behavior and mainly influencing the high-energy tail of the scaling function.

The 2p2h-MEC responses are calculated consistently with the mean field model in nuclear matter by introducing effective mass and vector energy for the nucleon, so they explicitly contain the same medium corrections as the quasielastic responses [29,30]. The contribution of the 2p2h tail has been obtained phenomenologically from (e, e') data through a pure phase-space model [31] similar to the one implemented in the GiBUU event generator [32], by a parameterization involving the phase-space function of the 2p2h process and the single-nucleon responses multiplied by a q-dependent 2p2h parameter. An additional improvement is that the single nucleon responses that are factorized in the scaling approach consist in an average with respect to a modified momentum distribution instead of extrapolations from the relativistic Fermi gas (RFG) model [31,33,34].

The SuSAM$*$+2p2h model was fitted to quasielastic electron data in Ref. [31] and therefore reproduces a large part of them (excluding inelastic and pion emission data). Here we intend to apply it to calculate the neutrino cross section to see what is achieved, as was done with the original SuSA model [35,36]. The SuSAM* model is based on the relativistic mean field model [37,38], and it provides an interesting alternative to the traditional SuSA model [20,39]. Indeed, the relativistic mean field is an optimal starting point for modeling the nuclear response, as it already adequately reproduces the position and width of the quasielastic peak with only two parameters; the Fermi momentum and the effective mass [37]. Besides it is relativistic, gauge invariant, and implicitly contains dynamical enhancement of lower Dirac components of the nucleon in the medium.

The structure of this work is as follows. In Sec. II we briefly describe the theoretical SuSAM$*$+2p2h model. In Sec. III we provide the results for the neutrino and antineutrino cross sections and compare with data. In Sec. IV we give our summary and conclusions.

II. FORMALISM

A. Response functions

In this work, our primary focus lies on studying inclusive charged-current quasielastic scattering (CCQE) of muon neutrinos from nuclei. In this section, we provide a concise overview of the formalism, which is elaborated in more detail in Refs. [31,40]. In the case of (ν_μ, μ^-) reaction the initial neutrino energy is denoted as $\epsilon = E_\nu$, and the final detected muon energy is represented as $\epsilon' = m_\mu + T_\mu$, where m_μ denotes the mass and T_μ is the kinetic energy of the muon.. The four-momentum transfer is defined as $Q^\mu = k^\mu - k'^\mu = (\omega, \mathbf{q})$, with $Q^2 = \omega^2 - q^2 < 0$, and the initial and final lepton momenta are k^μ and k'^μ. The scattering angle θ is given by $\mathbf{k} \cdot \mathbf{k}' = kk' \cos\theta$.

In this paper, our interest lies in the inclusive cross section, where only the final muon is detected. The cross section is expressed as follows:

$$\frac{d^2\sigma}{d\cos\theta dE_\mu} = \frac{G_F^2 \cos^2\theta_c}{2\pi} \frac{k'}{\epsilon} L_{\mu\nu} W^{\mu\nu}, \tag{1}$$

where G_F is the Fermi constant, θ_c is the Cabibbo angle, and $L_{\mu\nu}$ and $W^{\mu\nu}$ represent the leptonic and hadronic tensors, respectively. The leptonic tensor for neutrino scattering is given by

$$L_{\mu\nu} = k_\mu k'_\nu + k'_\mu k_\nu - g_{\mu\nu} k \cdot k' \pm i\epsilon_{\mu\nu\alpha\beta} k^\alpha k'^\beta, \tag{2}$$

where the sign $+(-)$ is for neutrino (antineutrino) scattering. The inclusive hadronic tensor is constructed from the matrix elements of the current operator $J^\mu(Q)$ between the initial and final hadronic states, summing over all the possible final nuclear states with excitation energy $\omega = E_f - E_i$, and averaging over the initial spin components.

$$W^{\mu\nu} = \sum_f \overline{\sum_i} \langle f|J^\mu(Q)|i\rangle^* \langle f|J^\nu(Q)|i\rangle \delta(E_i + \omega - E_f). \tag{3}$$

To express the cross section in a simple form in terms of response functions, we utilize the q-reference system where the momentum transfer $\mathbf{q}$ aligns with the z-axis, and the x-axis corresponds to the component perpendicular to q of the incident neutrino momentum. In this q-system, only the following five components of the hadronic tensor or response functions are involved:

$$R^{CC} = W^{00} \tag{4}$$

$$R^{CL} = -\frac{1}{2}(W^{03} + W^{30}) \tag{5}$$

$$R^{LL} = W^{33} \tag{6}$$

$$R^{T} = W^{11} + W^{22} \tag{7}$$

$$R^{T'} = -\frac{i}{2}(W^{12} - W^{21}). \tag{8}$$

B. Relativistic mean field

The SuSAM$*$+2p2h model considered in this work is based on the relativistic mean field model of nuclear matter, as initially proposed in Refs. [37,38,41,42]. In this model,

nucleons interact with a relativistic field characterized by scalar and vector potentials. The single-particle wave functions are described by plane waves with momentum $\mathbf{p}$, and their on shell energy is given by

$$E = \sqrt{(m_N^*)^2 + \mathbf{p}^2}, \tag{9}$$

where m_N^* represents the relativistic effective mass of the nucleon, defined as $m_N^* = m_N - g_s\phi_0 = M^* m_N$. Here, m_N denotes the bare nucleon mass, and $g_s\phi_0$ represents the scalar potential energy of the RMF [38]. Additionally, due to the repulsion by the relativistic vector potential, the nucleon acquires a positive energy given by $E_v = g_v V_0$. Hence, the total nucleon energy in the RMF model is the sum of the on-shell energy and the vector potential energy, $E_{\mathrm{RMF}} = E + E_v$. According to Ref. [29] we use the values $M^* = 0.8$ and $E_v = 141$ MeV for ^{12}C in our results.

In the RMF framework, the generic quasielastic responses with a one-body current operator can be expressed as follows:

$$R_{\mathrm{QE}}^K(q,\omega) = \frac{\epsilon_F - 1}{m_N^* \eta_F^3 \kappa} \mathcal{N} \bar{U}_K(q,\omega) f^*(\psi^*), \tag{10}$$

where $\mathcal{N} = Z, N$ for protons or neutrons responses, $\kappa = q/2m_N^*$ and $\eta_F = k_F/m_N^*$ are the Fermi energy and momentum, respectively, in units of the effective mass, with $E_F = \sqrt{k_F^2 + m_N^{*2}}$. The scaling variable $\psi^* = \psi^*(q,\omega)$ is related to the minimum energy of an on shell nucleon absorbing momentum q and energy ω,

$$\psi^* = \sqrt{\frac{\epsilon_0 - 1}{\epsilon_F - 1}} \mathrm{sgn}(\lambda - \tau), \tag{11}$$

where $\epsilon_F = E_F/m_N^*$ and

$$\epsilon_0 = \mathrm{Max}\left\{ \kappa\sqrt{1 + \frac{1}{\tau}} - \lambda, \epsilon_F - 2\lambda \right\}, \tag{12}$$

use the usual dimensionless variables normalized with m_N^*

$$\lambda = \omega/2m_N^*, \qquad \tau = \kappa^2 - \lambda^2. \tag{13}$$

Finally, the single nucleon functions $\bar{U}_K$ represent the responses of a single nucleon averaged in the Fermi gas [40].

In the RMF the scaling function is

$$f^*(\psi^*) = \frac{3}{4}(1 - \psi^{*2})\theta(1 - \psi^{*2}), \tag{14}$$

and therefore is zero outside the Fermi gas region $-1 < \psi^* < 1$. This is a consequence of the fact that nucleons have a maximum momentum k_F, which implies that, for a fixed q, there exists a maximum and minimum energy transfer where the response is nonzero.

C. Extended superscaling

In a finite nuclear system like an actual nucleus, the quasielastic response extends beyond the region $-1 < \psi^* < 1$. In the SuSAM* approach, the factorization, Eq. (10), remains intact, but using a phenomenological scaling function that is obtained from experimental data. As a result, the SuSAM* model can account for the complexities arising from finite nuclear systems and better describe the cross section. This extension also necessitates broadening the definition of the averaged single-nucleon responses beyond the RFG region, which can be achieved through a smearing of the Fermi surface, as implemented in [33,34]. In this context, we perform an averaging of the single-nucleon using the momentum distribution that is deduced from the scaling function. This procedure is elaborated upon in Appendix B of Ref. [31].

The first step in the scaling analysis involves subtracting the contribution of 2p2h MEC responses from the (e,e') data. The MEC responses are calculated in the RMF model of Ref. [29]. The experimental data of the scaling function, f_{exp}^*, are then obtained by dividing by the averaged single-nucleon cross section.

$$f_{\mathrm{exp}}^* = \frac{\left(\frac{d\sigma}{d\Omega d\omega}\right)_{\mathrm{exp}} - \left(\frac{d\sigma}{d\Omega d\omega}\right)_{\mathrm{MEC}}}{\sigma_M(v_L r_L + v_T r_T)}, \tag{15}$$

where σ_M is the Mott cross section, and the single nucleon dividing responses are such that the cancel with the factor multiplying the scaling function in Eq. (10)

$$r_K = \frac{\epsilon_F - 1}{m_N^* \eta_F^3 \kappa}(Z\bar{U}_K^p + N\bar{U}_K^n). \tag{16}$$

In this way the contamination arising from 2p2h-MEC response has been minimized to the greatest extent possible within the scaling data.

The process of selecting the QE-like data is essential for the SuSAM* approach, and it involves representing the f_{exp}^* data as a function of the scaling variable ψ^*. The data points belonging to the QE peak are expected to exhibit approximate scaling when plotted against ψ^*. While they may not align perfectly with the scaling function of the RFG, they predominantly cluster around a thick band near the RFG. On the other hand, data points corresponding to nonquasielastic processes like pion production clearly deviate from this band, scattering them in disparate points. This distinction enables the selection of QE-like data and the elimination of nonscaling inelastic data (approximately half of the ^{12}C dataset). The data selection process is formalized using a density algorithm; a data point is selected if it is surrounded by more than 25 points within

a radius $r = 0.1$. The density algorithm automatically identifies points that collapse into a dense region (scaling) and removes dispersed data points that do not collapse (nonscaling).

The selected QE-like data were used in Ref. [29] to construct a phenomenological SuSAM* scaling function, $f^*(\psi^*)$, which is parametrized as the sum of two Gaussians and exhibits a clear asymmetry around the origin $\psi^* = 0$, with a tail for $\psi^* > 0$. In Ref. [31], it was noticed that this tail is consistent with a contribution from 2p2h processes involving the one-body (OB) current. A significant portion of these effects could potentially originate from SRC that generate high-momentum nucleons in the ground state. Therefore, in the extended SuSAM* approach (ESuSAM*) an alternative parametrization of the phenomenological scaling function is proposed in the form

$$f^*_E(q,\omega) = f^*_{1p1h}(\psi^*) + f^*_{\mathrm{SRC}}(q,\omega), \tag{17}$$

where $f^*_{1p1h}(\psi^*)$ is a symmetric function that can be parametrized with a Gaussian

$$f^*_{1p1h}(\psi^*) = be^{-(\psi^*)^2/a^2}, \tag{18}$$

with the coefficients $a = 0.744$ and $b = 0.682$. The function $f^*_{\mathrm{SRC}}(q,\omega)$ characterizes the tail behavior of the scaling data for $\psi^* > 0$. It is formulated as a pure phase-space model (as shown below) because it is assumed to represent 2p2h contributions involving the OB current. This primarily includes SRC, interferences with MEC, and possibly other processes such as FSI. In other words, it cannot be solely attributed to SRC effects, even though we label it as such to differentiate it from the pure 2p2h MEC contribution.

In Fig. 1, we present the experimental QE scaling function data after subtracting the contribution of the tail, $f^*_{\mathrm{SRC}}(q,\omega)$. It is evident that the data now conforms to a band that aligns with a symmetric distribution, fitting well with a Gaussian centered at $\psi^* = 0$. This observation implies that the kinematic dependence of the tail, as modeled by the pure phase-space approach, is suitable for describing the high-energy tail accurately. The width of the band provides an indication of the extent to which the scaling hypothesis is violated.

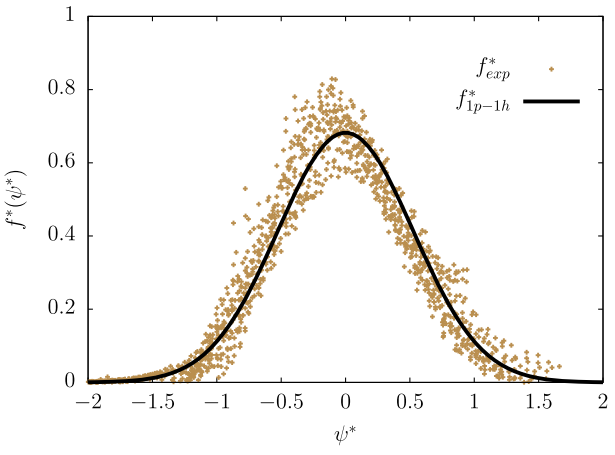

FIG. 1. The phenomenological scaling function used in this article compared to experimental data after subtracting the theoretical contribution of 2p2h.

Inserting the extended scaling function $f^*_E(q,\omega)$ in Eq. (10), the QE responses are the sum of two contributions

$$R^K_{\mathrm{QE}}(q,\omega) = R^K_{1p1h}(q,\omega) + R^K_{\mathrm{SRC}}(q,\omega), \tag{19}$$

where R^K_{1p1h} is proportional to $f^*_{1p1h}(\psi^*)$ and R^K_{SRC} is proportional to $f^*_{\mathrm{SRC}}(q,\omega)$ using Eq. (10). Thus, the former scales and the latter does not. However, in this model, both responses are proportional to the averaged single-nucleon response. The cross sections obtained using this ESuSAM* approach closely resemble those obtained with the original SuSAM* model, as both models have been fitted to the same dataset. However, the advantage of the extended model lies in its explicit ability to separate the contribution of the high-energy tail from the symmetric part of the scaling function, which lacks a tail. This feature becomes particularly useful in applications such as neutrino event generators, where distinguishing between different types of final states is essential. In the case of the R_{1p1h} response, the final states would be genuine 1p1h excitations, while for the R_{SRC} response, these states correspond to 2p2h excitations.

Finally the total responses in the ESuSAM$*$+MEC model are written as the sum of three contributions

$$R^K = R^K_{1p1h} + R^K_{\mathrm{SRC}} + R^K_{\mathrm{MEC}}. \tag{20}$$

The MEC contributions need to be added back because they were previously subtracted from the data to obtain the phenomenological scaling function $f^*(q,\omega)$. Note that pion emission and other inelastic channels are not included in this model.

D. Phase-space model

Next, we proceed to describe the pure phase space model for the SRC responses that contribute to the tail of the scaling function. The equations were derived in Ref. [31] from a factorized model for the emission of two correlated nucleons within the framework of the independent pair approximation. Subsequently, this factorized approximation was fitted to describe the tail of the phenomenological scaling function. The corresponding response functions for symmetric nuclei ($N = Z$) are the following:

$$R^K_{\rm SRC} = \frac{VF(q,\omega)}{(2\pi)^9}\frac{Z+\alpha(Z-1)}{2Z-1}\frac{c^{pn}(q)}{m_N^2 m_\pi^4}\bar{U}^K, \quad (21)$$

where $V/(2\pi)^3 = Z/(\frac{8}{3}\pi k_F^3)$.

In Eq. (21) the function $F(q,\omega)$ is the phase space function for the 2p2h excitations in the RMF model of nuclear matter

$$\begin{aligned} F(q,\omega) = \int d^3p_1' d^3p_2' d^3h_1 d^3h_2 \frac{(m_N^*)^4}{E_1 E_2 E_1' E_2'} \\ \times \theta(p_1'-k_F)\theta(k_F-h_1)\theta(p_2'-k_F)\theta(k_F-h_2) \\ \times \delta(E_1'+E_2'-E_1-E_2-\omega) \\ \times \delta(\mathbf{p}_1'+\mathbf{p}_2'-\mathbf{q}-\mathbf{h}_1-\mathbf{h}_2). \end{aligned} \quad (22)$$

In Eq. (21) the parameter $\alpha = 1/18$ take into account the dominance of np pairs over pp pairs in the high-momentum distribution, while the factor $[Z+\alpha(Z-1)]/(2Z-1)$ takes into account the percent contribution of pn, pp and nn pairs.

Finally, the coefficients $c^{\rm pn}(q)$ are the 2p2h parameters. The dividing factor $m_N^2 m_\pi^4$ is introduced for convenience so that the $c^{\rm pn}$ coefficients are adimensional. In the factorized independent-pair approximation the $c^{\rm pn}$ coefficients are proportional to the average value of the high-momentum distribution of a pn pair in the 2p2h excitation. In Ref. [31] the 2p2h parameters were fitted to describe the tail of the scaling function for each value of q. The q-dependence is well described by the approximate formula

$$c^{\rm pn}(q) = a_0\sqrt{\frac{m_N^*+q}{q}}\frac{m_N^*}{q} \quad (23)$$

with $a_0 = 345$.

The SRC response functions, Eq. (21) can be analytically evaluated using the frozen nucleon approximation in the phase-space function that can be approximated by a simple formula [43],

$$F(q,\omega) \simeq 4\pi\left(\frac{4}{3}\pi k_F^3\right)^2\frac{m_N^{*2}}{2}\sqrt{1-\frac{4m_N^{*2}}{(2m_N^*+\omega)^2-q^2}}, \quad (24)$$

This formula was utilized in Ref. [31] in the fit of the 2p2h coefficients. From this equation we obtain the minimum ω to excite a 2p2h state for fixed q, in frozen approximation, corresponding to the solution of $F(q,\omega)=0$

$$\omega_{\rm min} = \sqrt{4m_N^{*2}+q^2} - 2m_N^* \quad (25)$$

The phase-space function is set to zero below this value. Note that this is the kinetic energy of a particle with mass $2m_N^*$ and momentum q.

The factorization of Eq. (21) is similar to the pure phase-space model proposed in Ref. [44], with the distinction that our model incorporates an additional q-dependence in the 2p2h parameters. This extra q-dependence is necessary to accurately depict the tail of the scaling data in the quasielastic region [31].

E. Meson-exchange currents

The relativistic MEC model is adopted from Refs. [29,45], which builds upon the weak pion production model of Ref. [46]. This model encompasses the Feynman diagrams depicted in Fig. 2, categorized as seagull (a, b), pion-in-flight (c), pion-pole (d, e), and Δ (f–i) currents. Notably, the Δ current contribution proves to be the most significant within the momentum range of $q = 500$–1000 MeV/c, which holds utmost relevance for neutrino scattering.

The matrix elements of the MEC operator between the ground state and 2p2h excitations in the Fermi gas are given by

$$\begin{aligned} &\langle p_1' p_2' h_1^{-1} h_2^{-1}|J^\mu(Q)|F\rangle \\ &= \frac{(2\pi)^3}{V^2}\frac{(m_N^*)^2}{\sqrt{E_1 E_2 E_1' E_2'}} \\ &\quad \times \delta(\mathbf{p}_1'+\mathbf{p}_2'-\mathbf{q}-\mathbf{h}_1-\mathbf{h}_2) j^\mu(p_1', p_2', h_1, h_2), \end{aligned} \quad (26)$$

where the function $j^\mu(p_1', p_2', h_1, h_2)$ incorporates the spin and isospin indices of the Dirac spinors in the 2p2h excitation. The explicit expressions for these functions can be found in Ref. [29]. The 2p2h MEC responses are computed here within the framework of the RMF theory for nuclear matter. Consequently, the Dirac spinors are

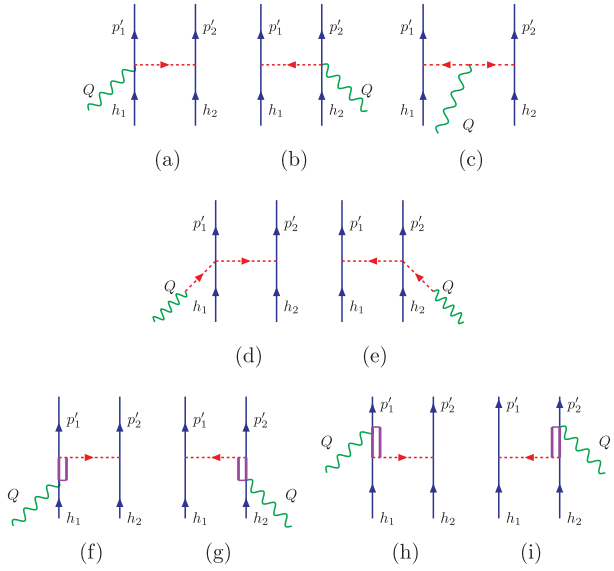

FIG. 2. Feynman diagrams for the electroweak MEC model used in this work.

associated with a relativistic effective mass m_N^*. The corresponding 2p2h hadronic tensor is computed as

$$W^{\mu\nu}_{\mathrm{MEC}} = \frac{V}{(2\pi)^9}\int d^3p_1' d^3p_2' d^3h_1 d^3h_2 \frac{(m_N^*)^4}{E_1 E_2 E_1' E_2'} \times w^{\mu\nu}(\mathbf{p}_1', \mathbf{p}_2', \mathbf{h}_1, \mathbf{h}_2)\delta(E_1' + E_2' - E_1 - E_2 - \omega) \times \theta(p_1' - k_F)\theta(k_F - h_1)\theta(p_2' - k_F)\theta(k_F - h_2) \times \delta(\mathbf{p}_1' + \mathbf{p}_2' - \mathbf{q} - \mathbf{h}_1 - \mathbf{h}_2), \quad (27)$$

where $V/(2\pi)^3 = Z/(\frac{8}{3}\pi k_F^3)$ for symmetric nuclear matter. The integral (26) in the nuclear hadronic tensor can be reduced to seven dimensions when calculating the response functions. The function $w^{\mu\nu}(\mathbf{p}_1', \mathbf{p}_2', \mathbf{h}_1, \mathbf{h}_2)$ represents the hadron tensor for single 2p2h transitions, summed up over spin and isospin,

$$w^{\mu\nu} = \frac{1}{4}\sum_{s_1 s_2 s_1' s_2'}\sum_{t_1 t_2 t_1' t_2'} j^\mu(p_1', p_2', h_1, h_2)^*_A j^\nu(p_1', p_2', h_1, h_2)_A, \quad (28)$$

where the two-body current matrix elements is conveniently antisymmetrized

$$j^\mu(p_1', p_2', h_1, h_2)_A \equiv j^\mu(p_1', p_2', h_1, h_2) - j^\mu(p_1', p_2', h_2, h_1) \quad (29)$$

and the factor $1/4$ in Eq. (28) accounts for the antisymmetry of the two-body wave function with respect to exchange of momenta, spin and isospin quantum numbers.

Due to the intricate nature of spin operators in the MEC, the summation over spin in Eq. (28) is numerically evaluated. Note that the single-nucleon tensor can be expanded as a sum of direct-direct, exchange-exchange, and direct-exchange interference terms. While in other models [18], the direct-exchange interference is not taken into account, the full contribution is included in our calculation.

III. RESULTS

In this section we present predictions of the ESuSAM $*$ +MEC model for neutrino and antineutrino CCQE. Our analysis involves a comparison with experimental data from MiniBooNE, T2K, and MINERvA collaborations. A novel aspect of our model is the inclusion, for the first time, of MEC two-nucleon emission computed within the framework of the RMF theory for nuclear matter. This approach accounts for dynamical effects in the MEC responses through the relativistic effective mass and vector energy of the nucleon.

While our approach shares similarities with the SuSAv2 + MEC model, which is widely used to study these reactions [20,47], it introduces significant differences in both the treatment of scaling and the handling of MEC.

The primary difference lies in the utilization of a unified analytical scaling function, derived from (e, e') data, and the inclusion of an averaged single-nucleon prefactor in our model. Additionally, the scaling variable in SuSAM* incorporates the effective mass of the nucleon. Another distinction is the decomposition of the scaling function into two parts; a symmetric function, $f^*_{\mathrm{1p1h}}(\psi^*)$, which represents the contribution of 1p1h processes, and a slightly scaling-violating function $f^*_{\mathrm{SRC}}(q, \omega)$, responsible for describing the tail of the scaling data. This latter function phenomenologically can account for 2p2h processes generated by interplay between one-body currents and correlated nucleon pairs, and interferences with MEC. Furthermore, in our model, the treatment of MEC involves the complete propagator of the Δ resonance, whereas the SuSAv2 + MEC model only includes the real part of the Δ propagator.

The parameters of the SuSAM* model (Fermi momentum $k_F = 225$ MeV/c, relativistic effective mass $M^* = 0.8$ and nucleon vector energy $E_v = 141$ MeV) are taken from Ref. [29]. The other input of the model is the phenomenological scaling function $f^*_E(q, \omega)$, extracted from (e, e') data as described in the previous section, and in more detail in Ref. [31].

A. MEC uncertainty

Before presenting the results for the neutrino cross sections, it is important to address the treatment of the Δ current in the MEC calculation. The Δ current introduces numerous uncertainties due to its model-dependent nature. Apart from the handling of the propagator, issues regarding form factors and the nuclear medium effect also arise. In this article, we do not delve deeply into all these complexities, as they are beyond the scope of this work. However, we will briefly discuss some of them.

One primary concern pertains to the axial form factor value for the excitation of the Δ at zero-momentum transfer which is commonly denoted as $C_5^A(0)$. A frequently accepted value that has been used in many calculations is $C_5^A(0) = 1.2$, which we employed in our previous works. However, in Ref. [46], this value was revisited through a more detailed analysis of weak pion emission by the nucleon, and it was revised downwards to $C_5^A(0) = 0.89$. This revised value is utilized in this work. We made this choice because, otherwise, the MEC response would be overly enhanced when compared with the data, as this value enters the calculations squared. The new value yields more reasonable results, as will be evident in the subsequent subsections. In Fig. 3, we contrast the computed transverse response using the two values $C_5^A(0) = 0.89$ and 1.2. It is evident that the response significantly increases with a larger axial form factor. Henceforth, all results presented utilize the smaller value 0.89.

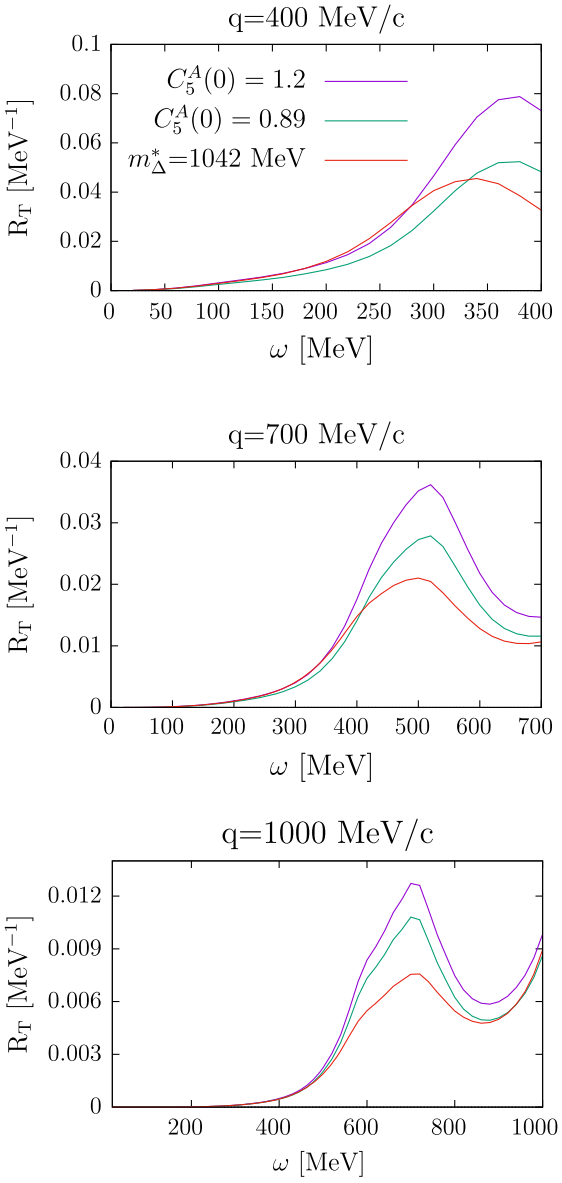

FIG. 3. Transverse MEC response employing three distinct prescriptions for the Δ current: (a) $C_5^A(0) = 1.2$, (b) $C_5^A = 0.89$, and (c) $m_\Delta^* = 1042$ MeV.

In this study, we do not account for modifications of the Δ within the nuclear medium; that is, we employ the Δ current in vacuum. Nonetheless, we can speculate about the implications of considering interactions between the Δ and the RMF. We suppose that, similar to the nucleon, the Δ may acquire an effective mass and vector energy due to these interactions. This topic was also addressed in Ref. [30], where an estimate of $M_\Delta^* = 1042$ MeV/c was proposed under the assumption of universal coupling, implying the same vector energy as the nucleon. This value is not firmly determined. Figure 2 presents an illustrative example of the transverse response when such Δ-medium interactions are taken into account. It is evident that the response experiences a reduction compared to the case of Δ in the vacuum.

Therefore, by examining the comparison of the transverse response in Fig. 2, which incorporates modifications to the axial form factor and interactions with the Δ in the medium, we can gauge the inherent uncertainty in the subsequent results regarding the MEC effects. This insight would suggest an uncertainty band for the 2p2h response on the order of ±20% at most due to these effects.

B. MiniBooNE

Here we present results for the kinematics of the (ν_μ, μ^-) reaction on ^{12}C as conducted in the MiniBooNE experiment, depicted in Fig. 4. In this experiment, the flux-averaged cross section was measured as a function of the muon energy for fixed values of $\cos\theta_\mu$. The kinematics in terms of T_μ (muon kinetic energy) and $\cos\theta_\mu$ (angle with respect to the incoming neutrino direction) are averaged over bins. The flux-averaged double differential cross section is computed as

$$\frac{d^2\sigma}{dT_\mu d\cos\theta_\mu} = \frac{\int dE_\nu \Phi(E_\nu) \frac{d^2\sigma}{dT_\mu d\cos\theta_\mu}(E_\nu)}{\int dE_\nu \Phi(E_\nu)}, \tag{30}$$

where $\Phi(E_\nu)$ is the neutrino flux and $\frac{d^2\sigma}{dT_\mu d\cos\theta_\mu}(E_\nu)$ is the cross section for fixed neutrino energy E_ν.

In Fig. 4, we show the individual contributions of the 1p1h responses (R_{1p1h}), the tail responses (R_{SRC}), and the 2p2h-MEC responses (R_{MEC}), as well as the total contribution obtained by summing these three components.

The computation of MEC responses entails intricate calculations, involving seven-dimensional integrals of the 2p2h responses. Additionally, there are integrations over neutrino energy for the flux-averaged cross section and possibly an additional averaging over bins in $\cos\theta_\mu$. To expedite these computations, a parametrization of the MEC responses was proposed in Ref. [30]. This parametrization introduces semiempirical formulas that factorize coupling coefficients, form factors, phase space, and the averaged Δ propagator. The semiempirical MEC formulas incorporate adjustable coefficients dependent on q, which are tabulated in [30]. This semiempirical approach proves highly advantageous, particularly due to its flexibility, enabling the modification of numerous model parameters without necessitating a readjustment of the coefficients. This flexibility may facilitate the study of systematic errors associated with the model parameters. In the case of the 1p1h and SRC responses, no such challenges are encountered, as they are represented by analytical functions.

The results presented in Fig. 4 are displayed in panels representing different bins of $\cos\theta_\mu$, where the flux-averaged cross section per neutron is plotted as a function of the muon kinetic energy T_μ. The width of the experimental bin is $\Delta\cos\theta_\mu = 0.1$. The results are shown as an

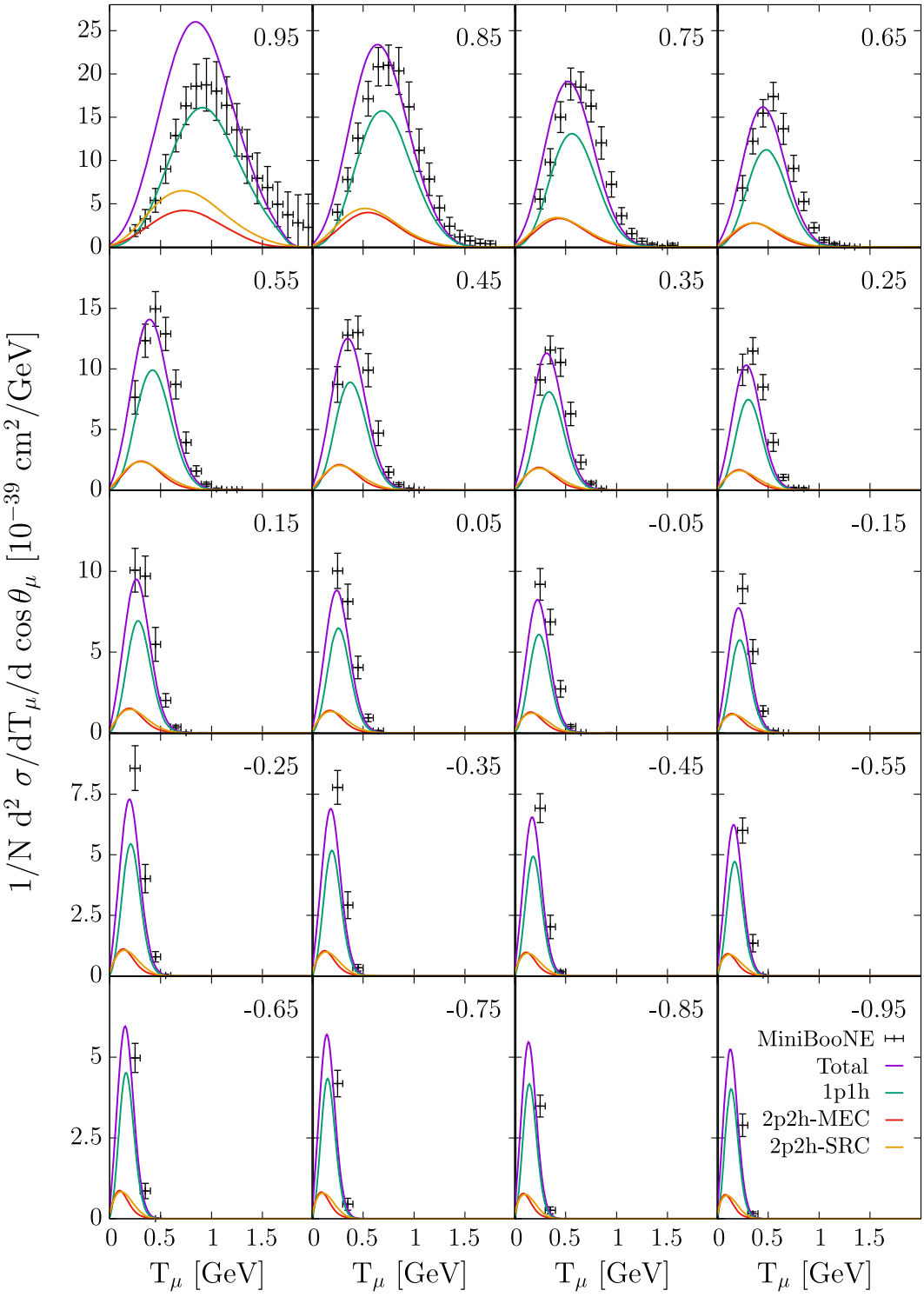

FIG. 4. Flux-integrated double-differential cross section for neutrino scattering on ^{12}C corresponding to the MiniBooNE experiment. The experimental data are from Ref. [48].

average over the bin, taking five equidistant points within each bin.

For extremely small angles, particularly $\cos\theta_\mu = 0.95$, our model clearly overestimates the data. In these cases, the transferred momentum (q) is also very small for the neutrinos that dominate the flux. For $q < 200$ MeV/c, the scaling model is not suitable due to the breakdown of the conditions required for the factorization approximation. At such small momenta, finite-size effects are important and the description of nuclear final states as plane waves is

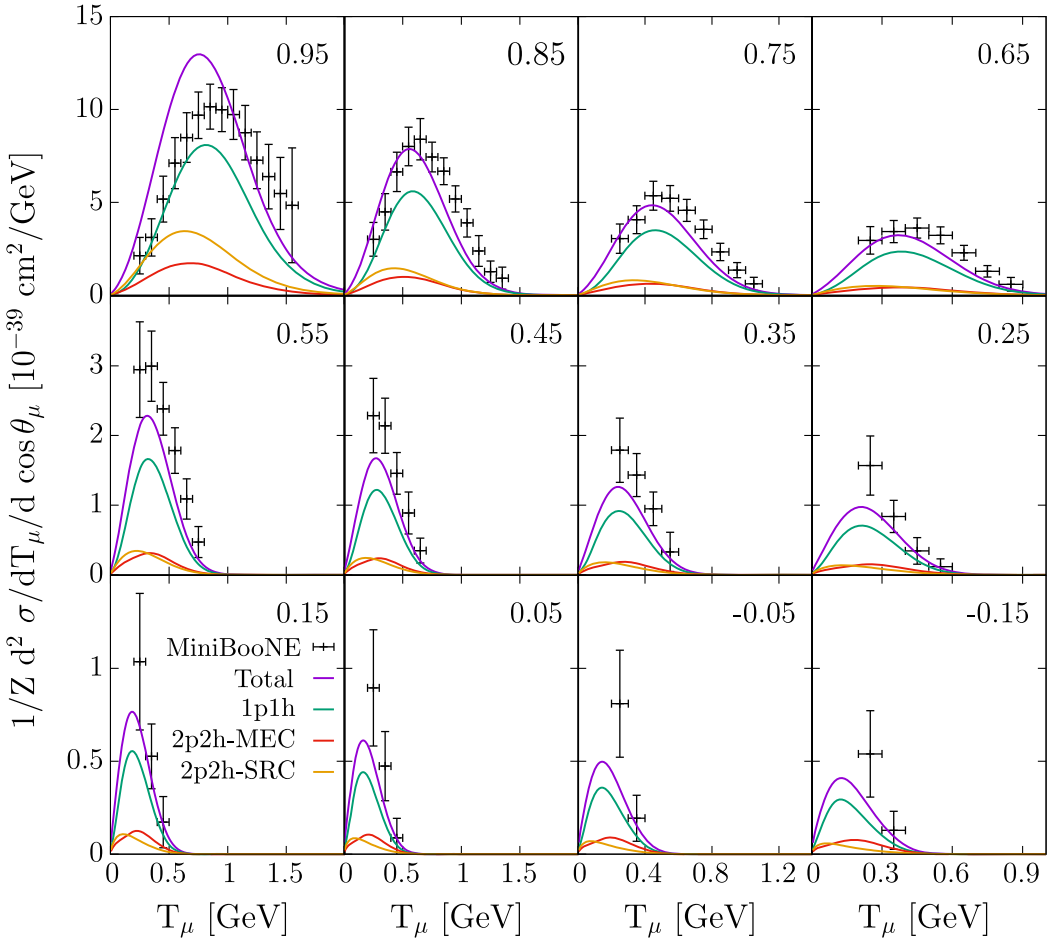

FIG. 5. MiniBooNE experiment flux-integrated double-differential cross section for antineutrino scattering on ^{12}C.The experimental data are from Ref. [49].

not valid. For larger scattering angles, the description of the data improves and is generally in agreement within the bounds of experimental error. However, a small shift of the data is observed compared to the theoretical distribution.

The impact of the MEC is nearly identical to that of the SRC, except once again for very small angles where the SRC effects are more pronounced. The peaks of the MEC and SRC responses almost coincide, with the maximum being shifted to lower energies compared to the peak of the 1p1h response. It is evident that the inclusion of both 2p2h contributions plays a significant role in accurately describing the observed data. The total effect of 2p2h contribution with respect to the total cross section is approximately 30%.

The antineutrino scattering case, as compared with MiniBooNE data, exhibits similar trends to the neutrino case, as shown in Fig. 5. In this case, the cross section averaged over flux is divided by the number of protons and plotted as a function of the muon's kinetic energy. For very small angles, the data are overestimated, as expected, and for larger angles, the description is reasonable, although generally, the data are underestimated. The effects of MEC and SRC correlations are comparable, except at very small angles where SRC dominates over MEC. However, this is again a regime where the model's validity is questionable. The overall impact of the 2p2h contribution amounts to approximately 30% of the total cross section.

We should clarify that the combined contributions referred to as 1p1h and SRC approximately coincide with the non-extended SuSAM* model employed in Ref. [50] for studying the same reaction. In that model, the scaling function was not decomposed into its symmetric and tail components. Given that both models were fitted to electron data, it is reasonable that they yield similar results by design. Our extended SuSAM* model holds the advantage of enabling the separation of the high-energy tail contribution from the scaling function, which is presumed to originate from the distribution of high momenta. Meanwhile, the 1p1h contribution corresponds to nucleons with moderate momenta.

On the other hand, the contribution of the MEC in the our approach is typically of a similar magnitude, to what was obtained in the SuSAv2 + MEC model [20,47]. The latter model neglected the imaginary part of the Δ propagator. In our current results, the complete propagator is

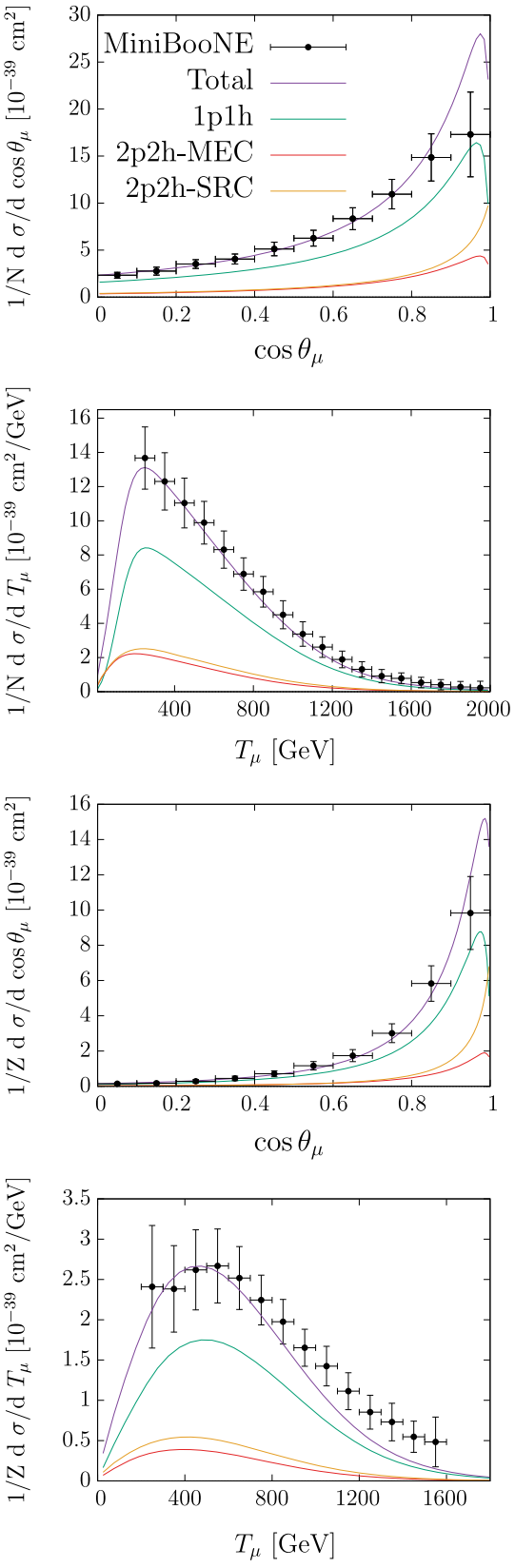

FIG. 6. MiniBooNE flux-averaged CCQE single-differential cross section as a function of $\cos\theta_\mu$ and T_μ for neutrino (top panels) and antineutrino scattering (bottom panels) from ^{12}C. The experimental data are from Refs. [48,49].

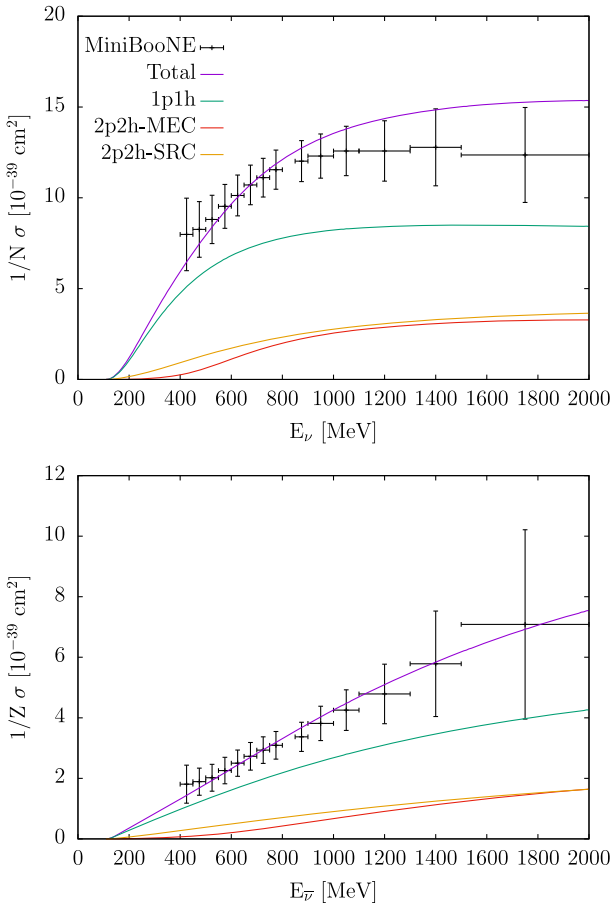

FIG. 7. MiniBooNE CCQE total neutrino (top panel) and atineutrino (bottom panel) cross section on ^{12}C. The experimental data are from [48,49].

employed, which tends to increase and shift the response to higher energies. However, the nucleons are described within the RMF framework, with effective mass and vector energy, leading to a reduction in the response. As a result, the combined effect yields responses of comparable magnitudes in both models. The quantitative differences between the two models were studied in Ref. [29].

In Fig. 6, a more comprehensive perspective of the previous results can be gained by integrating over $\cos\theta_\mu$ or T_μ to obtain the single-differential cross section with respect to T_μ or $\cos\theta_\mu$.

For neutrino scattering, the distribution in $\cos\theta_\mu$ is well-reproduced except at very forward angles, while the experimental T_μ distribution is accurately reproduced across all values. A similar conclusion can be drawn for antineutrino scattering, except that the T_μ distribution is slightly underestimated at high energies. In both cases, the contribution of 2p2h interactions proves essential to replicate the data.

Apart from the issues with very forward angles that have been previously mentioned, Fig. 6 highlights that the SRC response tends to increase significantly for $\cos\theta_\mu \sim 1$.

This effect is attributed to the extrapolation of the 2p2h parameter $c^{\mathrm{pn}}(q)$ to $q \to 0$, while the coefficients were fitted from $q = 100$ MeV/c onwards. These results can be improved by excluding the contributions from the SRC tail for q values less than 100 MeV/c, as their q-dependence becomes questionable in this region.

In Fig. 7, we present the MiniBooNE unfolded total cross section per neutron (proton) as a function of neutrino (antineutrino) energy The predictions from our comprehensive model align well with the data, although in the case of neutrino interaction, the prediction slightly exceeds the data, considering the error bars. The contributions from MEC and SRC are of comparable magnitude, each accounting for more than 20% of the total cross section.

Overall, our results do not significantly deviate from those of the SuSAv2 + MEC model. Therefore, the ESuSAM* model provides an alternative scaling plus 2p2h framework to describe the neutrino cross section. It is remarkable that the agreement of our results with the MiniBooNE data is similar to that obtained with more sophisticated models [19,51–54]. This is so because our model incorporates dynamic effects in the nucleon due to the RMF, like enhancement of transverse response due to lower components of nucleon spinors and other nuclear effects hidden into the phenomenological scaling function.

C. T2K

In Fig. 8, we depict the flux-folded CC double-differential cross-section for ν_μ-^{12}C scattering from the T2K experiment [55] in comparison with the predictions derived from the ESuSAM $*$ +MEC model. In this experiment, the bins in $\cos\theta_\mu$ possess a variable size. For larger angles, the bins are wider, while they become significantly smaller for smaller angles. This means that, for larger angles, we are averaging over a broader angular interval, thereby encompassing numerous values of q, which are generally large. This aligns

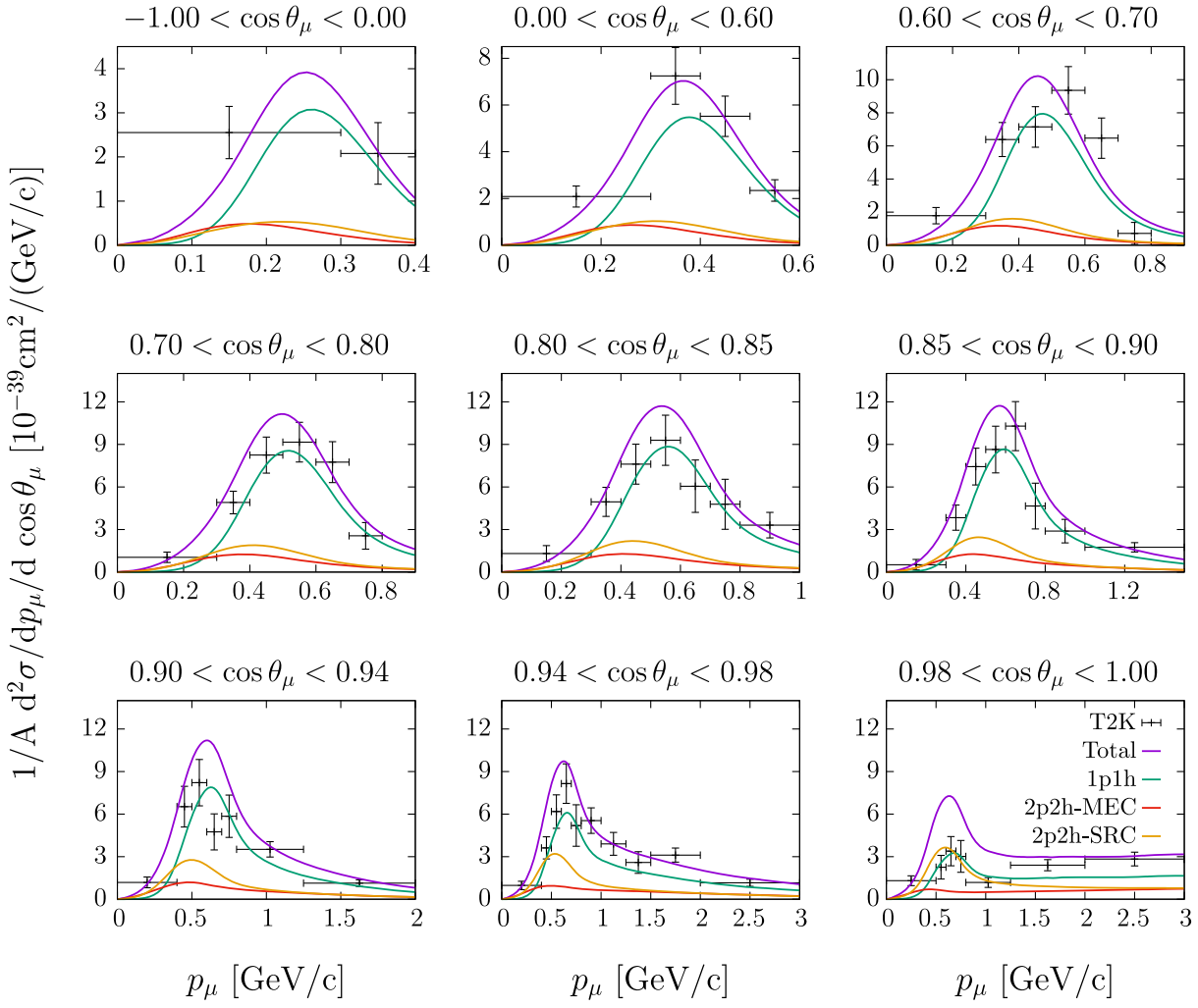

FIG. 8. T2K flux-folded double differential CCQE cross section per nucleon for ν_μ scattering on ^{12}C in the extended SuSAM $*$ +MEC model. Experimental data are from Ref. [55].

with the model's presumption of performing optimally at higher-q values.

It's important to note that the neutrino fluxes for T2K and MiniBooNE experiments are different, making the direct comparison of their results challenging. The T2K experiment utilizes a narrower neutrino flux centered around an energy of about 500 MeV, with an elongated tail. In contrast, the MiniBooNE experiment employs a broader and more uniform flux extending to energies of around 1.5 GeV. Consequently, different energy averages are being considered in these two experiments.

In general, our model reasonably reproduces the data, although it tends to slightly overestimate them as the $\cos\theta_\mu$ bin size increases. An exceptional case is observed in the bin $0.98 < \cos\theta_\mu < 1$, which corresponds to very forward angles. In this case, the model doubles the experimental cross section at the maximum, which corresponds to the lowest q region where the model's validity is questionable. However at this kinematics the tail of the cross section for high values of the muon momentum is well-reproduced.

Furthermore, the impact of the MEC is not as pronounced as observed in the MiniBooNE case, and its peak occurs at lower energies than the 1p1h response. This behavior is attributed to the emphasis of different regions in the flux average, where the MEC has less significance. The effect arising from the tail of the scaling function is similar to that of the MEC for larger angles but becomes more prominent as the angle decreases. It can be stated that for forward angles, the tail effect is increasingly emphasized. This emphasis reaches its zenith in the last bin, where the forward scattering is most significant. In this scenario, the SRC response is of similar magnitude as the 1p1h response. However, this

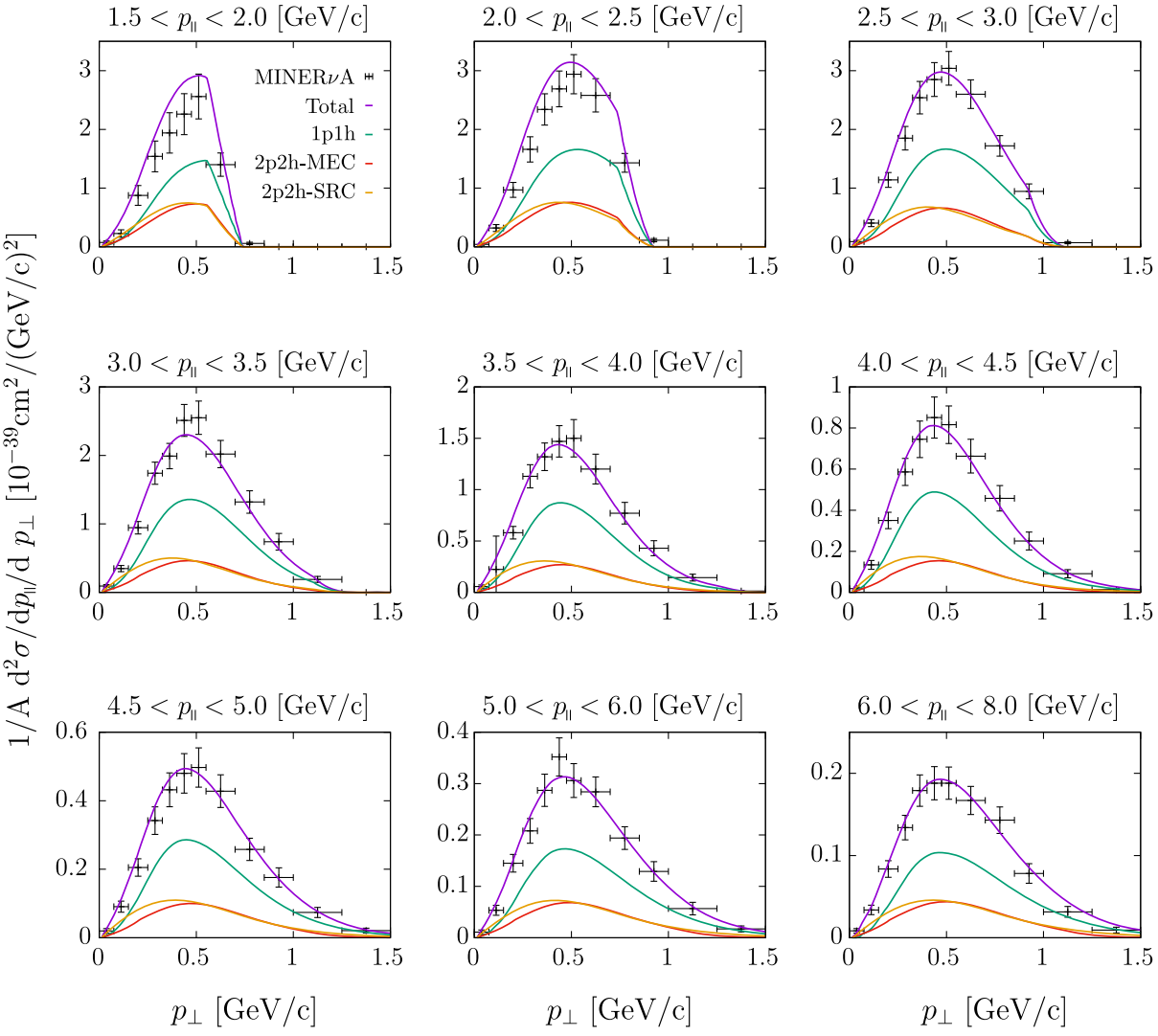

FIG. 9. MINERvA flux-folded double-differential cross section for muon neutrino scattering on hydrocarbon. The QE-like experimental data are from Ref. [7].

finding should be interpreted cautiously due to the intricate kinematic considerations involved in this regime.

D. MINERvA

The experimental data from MINERvA are provided as a function of the measured muon longitudinal and transverse momenta [7,8,56–59]. The double-differential cross section is expressed in terms of the longitudinal and transverse momenta of the scattered muon, denoted as $p_\parallel$ and $p_\perp$, respectively

$$p_\parallel = p_\mu \cos\theta_\mu, \qquad p_\perp = p_\mu \sin\theta_\mu.$$

These expressions establish the connection between the kinematic quantities in the context of the MINERvA experimental data, and there is the following relation between the cross sections in terms of both sets of variables:

$$\frac{d^2\sigma}{dp_\parallel dp_\perp} = \frac{\sin\theta_\mu}{E_\mu}\frac{d^2\sigma}{dE_\mu d\cos\theta_\mu}. \tag{31}$$

In Figs. 9 and 10 our results are compared with the QE-like data collected using a hydrocarbon target [7,8] for neutrino and antineutrino scattering, respectively. The computed flux-averaged cross sections and the MINERvA collaboration's data are in good agreement. Thanks to the high-energy neutrino flux, which can extend beyond 10 GeV, the involved momentum transfers are generally substantial, around 1 GeV/c, creating favorable kinematic conditions for the scaling model to describe the data.

Both the 2p2h contributions, including MEC and SRC, are of comparable magnitude, around 20% or more, and are crucial for capturing the data trends. The peaks of the 1p1h and 2p2h distributions practically coincide at the same value of $p_\perp$. The region where the extended SuSAM$*$+MEC model appears to struggle more is the first $p_\parallel$ bin,

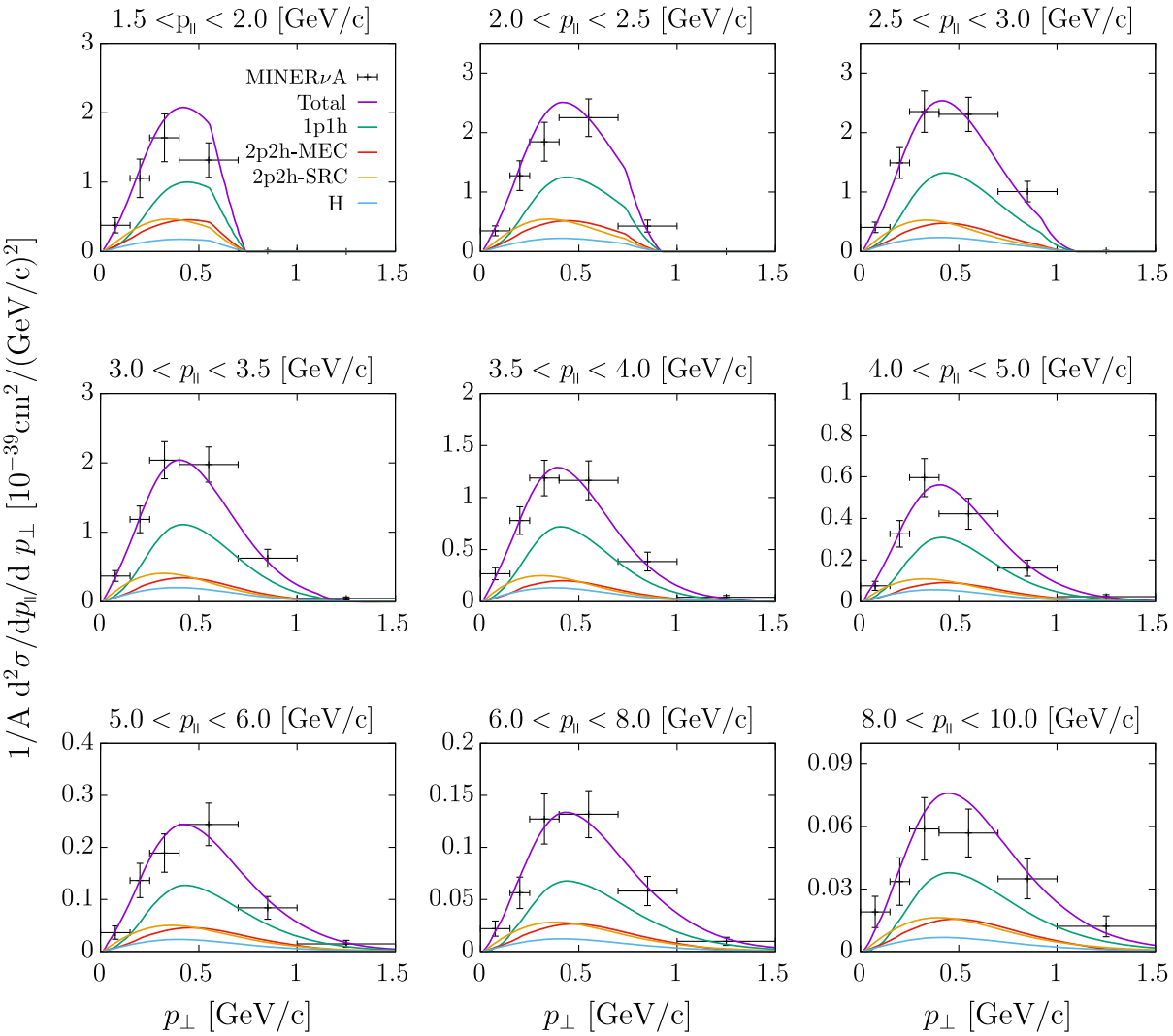

FIG. 10. MINERvA flux-folded double-differential cross section for antineutrino scattering on hydrocarbon. In antineutrino scattering, The single-nucleon contribution for the proton in H is also shown. The QE-like experimental data are from Ref. [8].

which corresponds to the lowest momentum transfer values, where the data are slightly overestimated for neutrino scattering on the left side of the curve. However, across the rest of the kinematics, the model aligns with the data within the error bars.

The strong agreement between the current model and the cross section data from the MINERvA experiment serves as a paradigmatic example. It demonstrates how a scaling model with 1p1h and 2p2h contributions derived from electron data can reproduce the neutrino cross section with only the modification of the current operator. This suggests that the more intricate aspects of nuclear structure relevant to the reaction are effectively incorporated implicitly within both the 1p1h and SRC scaling functions for the experiment's kinematics.

This outcome also represents a positive validation for the 2p2h MEC model based on the RMF framework, which encompasses dynamic components of nucleons within the nuclear medium. The successful agreement further reinforces the model's capability to describe neutrino interactions within these experimental conditions.

IV. CONCLUSIONS

In this study, we have employed an extended superscaling analysis with a relativistic effective mass to compute neutrino and antineutrino cross sections. Given that a significant source of systematic error in neutrino oscillation experiments arises from the lack of a complete theoretical description of neutrino-nucleus interactions, scaling-based models can offer valuable, alternative insights for such analyses. The scaling transformation can be regarded as an approximate symmetry of the nuclear response, yielding a universal function that solely depends on a scaling variable in the quasielastic regime. Changes in kinematics that keep the scaling variable invariant yield the same scaling function. In other words, different probes with distinct initial and final momentum transfers, k_i and k_f, expanding the same scaling variable, but exploring different (q, ω) spectral values, have the same scaled response.

The superscaling approach leverages the experimental scaling information obtained from quasielastic electron scattering to predict neutrino cross sections, assuming that the scaling function remains relatively insensitive to the specific type of lepton-nucleus interaction. This assumption allows for the extrapolation of the scaling function from electron scattering to neutrino interactions, providing a consistent framework to analyze and interpret neutrino-nucleus cross section data. By utilizing this approach, the theory-driven scaling function helps bridge the gap between different experimental measurements, providing a useful tool for understanding neutrino interactions across various experiments and energy ranges.

The extended SuSAM* approach employed in this study for (anti)neutrino scattering introduces several novel features and modifications. The scaling function is directly extracted from (e, e') data by subtracting the contribution of the 2p2h-MEC response and selecting quasielastic data points that collapse, while removing those that don't. Additionally, the phenomenological scaling function is decomposed into a sum of a symmetric function and the tail contribution, which is parametrized using a factorized 2p2h-like model.

The ESuSAM $*$ +MEC model relies on the RMF model of nuclear matter, a key feature that brings in dynamic relativistic ingredients. This sets it apart from the traditional approaches that often use the RFG model. The dynamic relativistic ingredients of the RMF, when applied to both the scaling function and the MEC, capture aspects of nucleon interactions that are crucial for understanding neutrino-nucleus interactions in a broader energy and momentum range.

The model includes three contributions: the 1p1h response, the 2p2h-MEC response and the 2p2h-SRC response. As a cautionary note, while SRC certainly contribute to the emission of two particles, the contribution referred to here as "2p2h-SRC" cannot be exclusively attributed to correlations alone. This is because correlations cannot be disentangled from other effects that also contribute to the tail of the scaling function, such as interference with MEC, final-state interactions, and other ingredients that violate scaling. At best, it can be said that this contribution serves as an upper limit for the effects of SRC on the nuclear response. In any case, it is useful to decompose the results into the genuine contribution from 1p1h emission and the contribution from the tail, which is compatible with 2p2h events. By distinguishing between these contributions, the model provides a more nuanced understanding of the underlying nuclear dynamics and the various factors that contribute to the observed responses in neutrino scattering.

By utilizing this framework, we have successfully reproduced a wide range of experimental data from MiniBooNE, T2K, and MINERvA Collaborations. The fact that the model performs well, especially at higher-momentum transfers, indicates that it captures the underlying physics of neutrino-nucleus interactions in those regimes. The challenges arise when dealing with very low-momentum transfers, where the model's predictions deviate from the data. This is not uncommon, as the theoretical description of very low momentum transfers can be complex due to effects like nuclear-shell structure and the limitations of the model assumptions. Using a shell-model approach for low q is more reasonable, as shell models are better suited for describing the behavior of nucleons in those energy regimes.

The significant contribution of the 2p2h response to the overall response, particularly for experiments with higher momentum transfers like MINERvA, underscores the

importance of considering multinucleon emission in neutrino-nucleus interactions. The comparable impact of MEC and SRC effects further emphasizes their significant roles in the response, which is consistent with the complexity of these interactions.

This extension of the SuSAM* model, along with its successful comparison to data, not only provides valuable insights into neutrino interactions but also underlines the significance of considering dynamic nucleon effects within the nuclear medium. These findings emphasize the potential of scaling-based models to contribute to a deeper understanding of neutrino-nucleus interactions and their implications for neutrino oscillation experiments.

ACKNOWLEDGMENTS

This work is supported by Grant No. PID2020–114767GB-I00 funded by MCIN/AEI/10.13039/501100011033; FEDER/Junta de Andalucia-Consejeria de Transformacion Economica, Industria, Conocimiento y Universidades/A-FQM-390-UGR20; Junta de Andalucia (Grant No. FQM-225).

[1] A. B. Balantekin, S. Gardiner, K. Mahn, T. Mohayai, J. Newby, V. Pandey, J. Zettlemoyer, J. Asaadi, M. Betancourt, D. A. Harris *et al.*, arXiv:2209.06872.
[2] K. Abe *et al.* (T2K Collaboration), Nature (London) **580**, 339 (2020); **583**, E16 (2020).
[3] U. Mosel, Annu. Rev. Nucl. Part. Sci. **66**, 171 (2016).
[4] T. Katori and M. Martini, J. Phys. G **45**, 013001 (2018).
[5] L. Alvarez-Ruso *et al.*, Prog. Part. Nucl. Phys. **100**, 1 (2018).
[6] A. M. Ankowski, A. Ashkenazi, S. Bacca, J. L. Barrow, M. Betancourt, A. Bodek, M. E. Christy, L. D. S. Dytman, A. Friedland, O. Hen *et al.*, J. Phys. G **50**, 120501 (2023).
[7] D. Ruterbories *et al.* (MINERvA Collaboration), Phys. Rev. D **99**, 012004 (2019).
[8] C. E. Patrick *et al.* (MINERvA Collaboration), Phys. Rev. D **97**, 052002 (2018).
[9] K. Abe *et al.* (T2K Collaboration), Nucl. Instrum. Methods Phys. Res., Sect. A **659**, 106 (2011).
[10] K. Abe *et al.* (T2K Collaboration), Phys. Rev. D **98**, 012004 (2018).
[11] K. Abe *et al.* (T2K Collaboration), Phys. Rev. D **98**, 032003 (2018).
[12] P. Adamson *et al.* (NOvA Collaboration), Phys. Rev. Lett. **116**, 151806 (2016).
[13] R. Acciarri *et al.* (DUNE Collaboration), arXiv:1512.06148.
[14] O. Palamara (ArgoNeuT Collaboration), J. Phys. Soc. Jpn. Conf. Proc. **12**, 010017 (2016).
[15] R. Acciarri *et al.* (ArgoNeuT Collaboration), Phys. Rev. D **90**, 012008 (2014).
[16] A. R. Back *et al.* (ANNIE Collaboration), arXiv:1707.08222.
[17] M. Martini, M. Ericson, G. Chanfray, and J. Marteau, Phys. Rev. C **80**, 065501 (2009).
[18] J. Nieves, I. Ruiz Simo, and M. J. Vicente Vacas, Phys. Rev. C **83**, 045501 (2011).
[19] K. Gallmeister, U. Mosel, and J. Weil, Phys. Rev. C **94**, 035502 (2016).
[20] G. D. Megias, J. E. Amaro, M. B. Barbaro, J. A. Caballero, T. W. Donnelly, and I. Ruiz Simo, Phys. Rev. D **94**, 093004 (2016).
[21] N. Rocco, A. Lovato, and O. Benhar, Phys. Rev. Lett. **116**, 192501 (2016).
[22] M. Martini, N. Jachowicz, M. Ericson, V. Pandey, T. Van Cuyck, and N. Van Dessel, Phys. Rev. C **94**, 015501 (2016).
[23] J. E. Amaro, E. Ruiz Arriola, and I. Ruiz Simo, Phys. Rev. C **92**, 054607 (2015).
[24] J. E. Amaro, E. Ruiz Arriola, and I. Ruiz Simo, Phys. Rev. D **95**, 076009 (2017).
[25] W. M. Alberico, A. Molinari, T. W. Donnelly, E. L. Kronenberg, and J. W. Van Orden, Phys. Rev. C **38**, 1801 (1988).
[26] D. B. Day, J. S. McCarthy, T. W. Donnelly, and I. Sick, Annu. Rev. Nucl. Part. Sci. **40**, 357 (1990).
[27] T. W. Donnelly and I. Sick, Phys. Rev. C **60**, 065502 (1999).
[28] J. E. Amaro, M. B. Barbaro, J. A. Caballero, T. W. Donnelly, R. Gonzalez-Jimenez, G. D. Megias, and I. R. Simo, Eur. Phys. J. Spec. Top. **230**, 4321 (2021).
[29] V. L. Martinez-Consentino, I. R. Simo, and J. E. Amaro, Phys. Rev. C **104**, 025501 (2021).
[30] V. L. Martinez-Consentino, J. E. Amaro, and I. Ruiz Simo, Phys. Rev. D **104**, 113006 (2021).
[31] V. L. Martinez-Consentino, J. E. Amaro, P. R. Casale, and I. Ruiz Simo, Phys. Rev. D **108**, 013007 (2023).
[32] U. Mosel, O. Lalakulich, and K. Gallmeister, Phys. Rev. D **89**, 093003 (2014).
[33] P. R. Casale, J. E. Amaro, V. L. Martinez-Consentino, and I. Ruiz Simo, Universe **9**, 158 (2023).
[34] P. R. Casale, J. E. Amaro, and M. B. Barbaro, Symmetry **15**, 1709 (2023).
[35] J. E. Amaro, M. B. Barbaro, J. A. Caballero, T. W. Donnelly, A. Molinari, and I. Sick, Phys. Rev. C **71**, 015501 (2005).
[36] J. E. Amaro, M. B. Barbaro, J. A. Caballero, T. W. Donnelly, and C. Maieron, Phys. Rev. C **71**, 065501 (2005).
[37] R. Rosenfelder, Ann. Phys. (N.Y.) **128**, 188 (1980).
[38] B. D. Serot and J. D. Walecka, in *Advances in Nuclear Physics*, edited by J. W. Negele and E. Vogt (Plenum, New York, 1986), Vol. 16.
[39] G. D. Megias, M. B. Barbaro, J. A. Caballero, J. E. Amaro, T. W. Donnelly, I. Ruiz Simo, and J. W. Van Orden, J. Phys. G **46**, 015104 (2019).
[40] J. E. Amaro, M. B. Barbaro, J. A. Caballero, R. González-Jiménez, G. D. Megias, and I. Ruiz Simo, J. Phys. G **47**, 124001 (2020).
[41] K. Wehrberger, Phys. Rep. **225**, 273 (1993).

[42] M. B. Barbaro, R. Cenni, A. De Pace, T. W. Donnelly, and A. Molinari, Nucl. Phys. A **A643**, 137 (1998).
[43] I. Ruiz Simo, C. Albertus, J. E. Amaro, M. B. Barbaro, J. A. Caballero, and T. W. Donnelly, Phys. Rev. D **90**, 053010 (2014).
[44] O. Lalakulich, K. Gallmeister, and U. Mosel, Phys. Rev. C **86**, 014614 (2012); **90**, 029902(E) (2014).
[45] I. Ruiz Simo, J. E. Amaro, M. B. Barbaro, A. De Pace, J. A. Caballero, and T. W. Donnelly, J. Phys. G **44**, 065105 (2017).
[46] E. Hernandez, J. Nieves, and M. Valverde, Phys. Rev. D **76**, 033005 (2007).
[47] G. D. Megias, M. B. Barbaro, J. A. Caballero, J. E. Amaro, T. W. Donnelly, I. Ruiz Simo, and J. W. Van Orden, J. Phys. G **46**, 015104 (2019).
[48] A. A. Aguilar-Arevalo *et al.* (MiniBooNE Collaboration), Phys. Rev. D **81**, 092005 (2010).
[49] A. A. Aguilar-Arevalo *et al.* (MiniBooNE Collaboration), Phys. Rev. D **88**, 032001 (2013).
[50] I. Ruiz Simo, V. L. Martinez-Consentino, J. E. Amaro, and E. Ruiz Arriola, Phys. Rev. D **97**, 116006 (2018).
[51] J. Nieves, I. Ruiz Simo, and M. J. Vicente Vacas, Phys. Lett. B **707**, 72 (2012).
[52] J. Nieves, I. Ruiz Simo, and M. J. Vicente Vacas, Phys. Lett. B **721**, 90 (2013).
[53] M. Martini, M. Ericson, and G. Chanfray, Phys. Rev. C **84**, 055502 (2011).
[54] M. Martini and M. Ericson, Phys. Rev. C **87**, 065501 (2013).
[55] K. Abe *et al.* (T2K Collaboration), Phys. Rev. D **93**, 112012 (2016).
[56] M. Betancourt, J. Phys. Soc. Jpn. Conf. Proc. **12**, 010016 (2016).
[57] X.-G. Lu, Z. A. Dar, F. Akbar *et al.* (The MINERvA Collaboration), Eur. Phys. J. Spec. Top. **230**, 4243 (2021).
[58] D. Ruterbories *et al.* (The MINERvA Collaboration), Phys. Rev. D **104**, 092010 (2021).
[59] J. Kleykamp *et al.* (MINERvA Collaboration), Phys. Rev. Lett. **130**, 161801 (2023).